iJRASET
International Journal For Research in Applied Science and Engineering Technology

INTERNATIONAL JOURNAL FOR RESEARCH

IN APPLIED SCIENCE & ENGINEERING TECHNOLOGY

Volume: 14 **Issue:** III **Month of publication:** March 2026

DOI: https://doi.org/10.22214/ijraset.2026.79141

www.ijraset.com

Call: 08813907089 | E-mail ID: ijraset@gmail.com

International Journal for Research in Applied Science & Engineering Technology (IJRASET)
ISSN: 2321-9653; IC Value: 45.98; SJ Impact Factor: 7.538
Volume 14 Issue III Mar 2026- Available at www.ijraset.com

Green Synthesis, Characterization and Applications of Magnesium Oxide Nanoparticles Using *Terminalia Arjuna* Bark and *Coriandrum Sativum* Seed Extracts

Vincy S[1], Dr. G. Savari Susila[2]
[1]*Department of PG Chemistry (SSC), St. Mary's College (Autonomous), Thoothukudi 628001,Affiliated to Manonmaniam Sundaranar University, Tirunelveli,Tamil Nadu, India*
[2]*Department of PG Chemistry (SSC), St. Mary's College (Autonomous), Thoothukudi 628001, Affiliated to Manonmaniam Sundaranar University, Tirunelveli, Tamil Nadu, India*

Abstract: ***Magnesium oxide nanoparticles (MgO NPs) were synthesized using an eco-friendly green chemistry approach employing* Terminalia arjuna *bark extract and* Coriandrum sativum *seed extract as natural reducing and stabilizing agents. The phytochemicals present in the plant extracts facilitated nanoparticle formation without the use of toxic chemicals. The synthesized nanoparticles were characterized using UV–Visible spectroscopy, FTIR, XRD, FESEM, EDAX, and TGA techniques. UV–Visible spectra confirmed nanoparticle formation, while FTIR analysis indicated the involvement of hydroxyl and carbonyl functional groups in reduction and stabilization. XRD patterns revealed highly crystalline cubic MgO with nanoscale crystallite size. FESEM images showed quasi-spherical agglomerated nanoparticles, and EDAX confirmed the presence of Mg and O elements, indicating high purity. TGA analysis demonstrated good thermal stability. The synthesized MgO nanoparticles exhibited significant antibacterial activity against Gram-positive and Gram-negative bacteria. MgO-coated metal specimens showed improved corrosion resistance in acidic, basic, and neutral media. Additionally, edible coating applications delayed ripening, reduced microbial spoilage, and maintained firmness during storage. The results highlight the potential of plant-mediated MgO nanoparticles for sustainable synthesis, antimicrobial applications, corrosion protection, and post-harvest food preservation.***

Keywords: Green synthesis, MgO nanoparticles, Antibacterial activity, Corrosion resistance, Food preservation.

I. INTRODUCTION

Nanotechnology has rapidly developed in recent years, focusing on materials at the nanoscale range (1–100 nm) [1]. Metal oxide nanoparticles such as magnesium oxide (MgO), zinc oxide (ZnO), and copper oxide (CuO) have gained considerable attention due to their unique physicochemical properties, including high surface area, enhanced reactivity, and improved biological activity, making them suitable for biomedical, environmental, and catalytic applications [2].

Conventional nanoparticle synthesis methods often involve toxic chemicals, high energy consumption, and complex procedures, which may lead to environmental and health concerns [3]. To overcome these limitations, green synthesis has emerged as an eco-friendly and sustainable alternative that utilizes biological sources such as plant extracts, microorganisms, and enzymes for nanoparticle production [4].Plant-mediated synthesis is particularly advantageous due to the presence of phytochemicals such as flavonoids, phenolics, alkaloids, and terpenoids, which act as reducing and stabilizing agents during nanoparticle formation [5]. Terminalia arjuna bark contains bioactive compounds with antioxidant and antimicrobial properties, making it suitable for green synthesis [6]. Similarly, Coriandrum sativum seeds contain essential oils and phenolic compounds that enhance nanoparticle formation and stability [7].

Green-synthesized nanoparticles exhibit improved biocompatibility and environmental safety, with promising applications in antimicrobial, antioxidant, and environmental remediation fields [8,9]. Therefore, the present study focuses on the eco-friendly synthesis of metal oxide nanoparticles using Terminalia arjuna bark and Coriandrum sativum seeds as natural reducing agents.

II. LITERATURE REVIEW

Ashok Kumar et al. (2022) developed magnesium oxide nanoparticles using Camellia sinensis extract through a simple green synthesis method. The synthesized nanoparticles exhibited a well-defined cubic crystalline structure confirmed by XRD analysis. Structural parameters were further evaluated using Williamson–Hall analysis. The synthesized MgO nanoparticles demonstrated excellent photocatalytic activity with approximately 97% degradation efficiency of methylene blue dye, highlighting their potential for wastewater treatment applications [96].

Rajiv Periakaruppan and V. Naveen (2022) synthesized MgO nanoparticles using Piper nigrum leaf extract. The obtained nanoparticles showed rod-like morphology with an average particle size of around 20 nm. Antioxidant studies revealed strong free radical scavenging activity, where higher concentrations showed significant antioxidant efficiency. These findings suggested that the synthesized MgO nanoparticles could be useful for biomedical and pharmaceutical applications [97].

Hanif Amrulloh et al. (2021) reported green synthesis of MgO nanoparticles using Moringa oleifera bark extract. The formation of nanoparticles was confirmed through UV–Visible spectroscopy and XRD analysis. The synthesized particles were spherical in shape with sizes ranging from 60–100 nm. The nanoparticles exhibited notable antioxidant properties and effective antibacterial activity against both Gram-positive and Gram-negative bacterial strains [98].

Mary Harli Mol Edwin et al. (2024) synthesized MgO nanoparticles using Vitis vinifera extract through a green synthesis approach. Morphological studies revealed uniformly distributed spherical nanoparticles with microporous structures. The synthesized nanoparticles demonstrated multiple biological activities including antibacterial, antifungal, anti-inflammatory, and anti-diabetic properties, indicating their potential biomedical applications [99].

III. METHODOLOGY

A. *Green Synthesis of Mgo Nanoparticles using* TERMINALIA ARJUNA

1) *Collection of Plant Material*

Terminalia arjuna bark was collected from St. Mary's College campus, Thoothukudi. The collected bark was washed thoroughly with distilled water to remove impurities and dried in dark conditions at room temperature for about 15 days. The dried bark was then powdered and stored for further use.

2) *Preparation of Bark Extract*

About 5 g of powdered bark was added to 100 mL distilled water and boiled for 30 minutes. The mixture was cooled and filtered to obtain a clear extract. The extract contains phytochemicals such as flavonoids, phenolics, and tannins, which act as reducing and stabilizing agents.

Fig. 4.2 Preparation of *Terminalia arjuna* Bark Extract

3) Synthesis of MgO Nanoparticles

For synthesis, 10 mL of 0.1 M $Mg(NO_3)_2$ solution was mixed with 40 mL of bark extract and stirred for 45 minutes. Then, 0.2 M NaOH solution was added dropwise to form a precipitate. The obtained precipitate was washed, dried, and calcined at 873 K for 4 hours to obtain MgO nanoparticles. The sample was labeled as MgO–T.

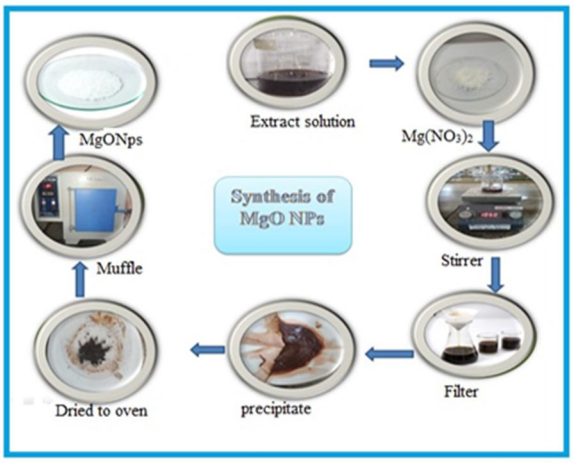

Fig. 4.3 Synthesis of *Terminalia arjuna* Mediated MgO Nps

B. Green synthesis of Mgo nanoparticles using Coriandrum Sativum

1) Preparation of Seed Extract

Coriandrum sativum seeds were purchased from a local market in Thoothukudi. About 50 g of seeds were washed, soaked overnight in deionized water, and crushed using a grinder. The extract was filtered, diluted to 250 mL, and stored at 4 °C for further use.

2) Synthesis of MgO Nanoparticles

A 0.1 M $Mg(NO_3)_2$ solution (100 mL) was prepared, and 50 mL of seed extract was added dropwise under constant stirring. A brown precipitate formed immediately, indicating nanoparticle formation. The precipitate was washed with alcohol, dried in a hot air oven, and powdered to obtain MgO nanoparticles. The sample was labeled as MgO–C.

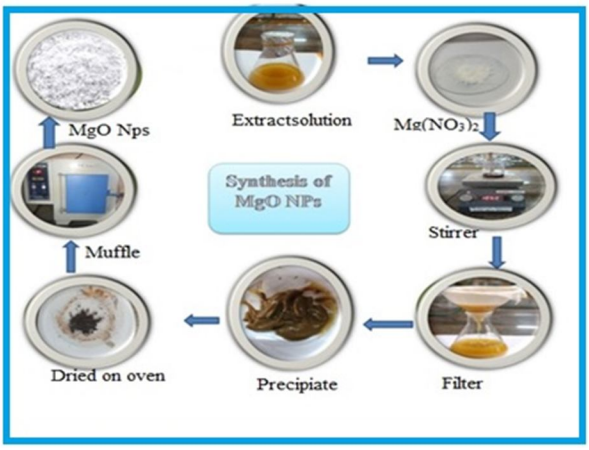

Fig 4.5 Schematic representation of the Synthesis of *coriandrum sativum seeds extract* Assisted MgO NPs

IV. RESULTS AND DISCUSSION

A. Characteristics of MgO–C and MgO -T Nanoparticles

1) UV–Visible Analysis of Green Synthesized MgO–C and MgO–T Nanoparticles

The UV–Visible spectra of green synthesized MgO–C and MgO–T nanoparticles were recorded to study their optical properties and confirm nanoparticle formation. The MgO–C nanoparticles exhibited absorption peaks at 266 nm and 329 nm, as shown in Fig. 4.1. The peak at 266 nm is attributed to π–π* transition of phytochemicals and band-to-band electronic transition of MgO nanoparticles,

confirming nanoscale formation. The absorption peak at 329 nm is assigned to n–π* transition and metal–oxygen charge transfer, which arise due to surface defects, oxygen vacancies, and phytochemical capping [10–12].

Similarly, the UV–Visible spectrum of MgO–T nanoparticles showed characteristic absorption peaks at 367.8 nm and 395.1 nm, as illustrated in Fig. 4.2. These peaks correspond to n–π* transition and metal–oxygen charge transfer transitions caused by surface functional groups and phytochemicals from *Terminalia arjuna* bark extract. Additionally, weak absorption bands observed at 848.9 nm and 1079.1 nm are attributed to defect-related states and charge transfer transitions due to oxygen vacancies and surface imperfections. These results confirm the successful formation and enhanced optical properties of green synthesized MgO–T nanoparticles [13–15].

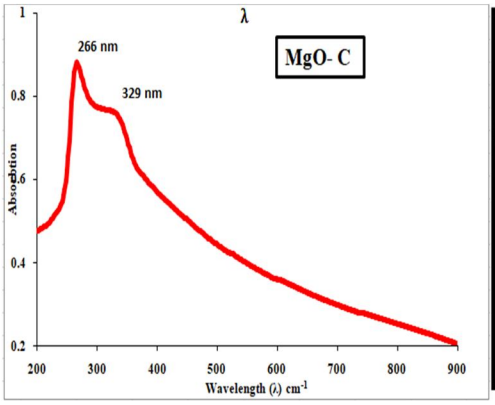

Fig. 4.1 UV–Vis Spectrum of MgO–CNPS

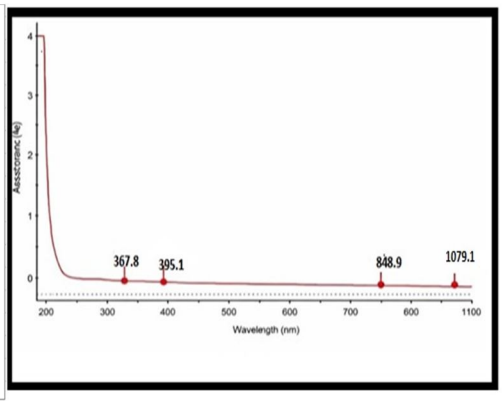

Fig. 4.2 UV–Visible Spectrum of MgO–T Nps

2) FTIR Spectral Analysis of MgO–C and MgO–T Nanoparticles

The FTIR spectrum of MgO–C nanoparticles (Fig. 4.3) shows a broad peak at 3348–3323 cm^{-1} corresponding to O–H stretching vibrations of phytochemicals. The peaks at 2935–2923 cm^{-1} and 1643–1561 cm^{-1} are attributed to C–H and C=O stretching vibrations, indicating the involvement of plant biomolecules in nanoparticle stabilization. The bands at 1103–1011 cm^{-1} correspond to C–O stretching, while the peaks at 866–851 cm^{-1}, 560 cm^{-1} and 474 cm^{-1} represent metal–oxygen (Mg–O) stretching vibrations, confirming MgO nanoparticle formation [10–12].

The FTIR spectrum of MgO–T nanoparticles (Fig. 4.4) exhibits O–H stretching vibrations at 3420–3500 cm^{-1} and C–H stretching at 2920–2850 cm^{-1}. The band at 1630–1650 cm^{-1} corresponds to C=O stretching, and the peak at 1400–1450 cm^{-1} indicates C–N stretching vibrations from plant metabolites. The strong band around 500–600 cm^{-1} corresponds to metal–oxygen (Mg–O) stretching, confirming successful formation of MgO nanoparticles through green synthesis [11–14].

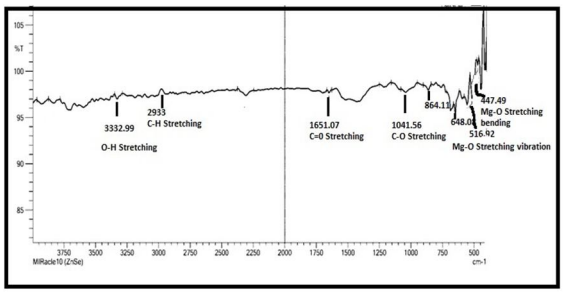

Fig 4.3 FTIR Spectrum of MgO–C Nps

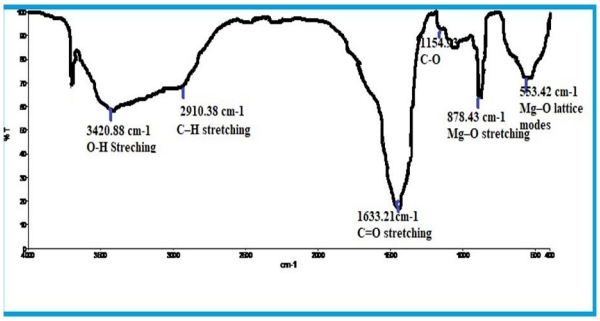

Fig 4.4 FTIR Spectrum of MgO–T Nps

3) XRD Analysis of Green Synthesized MgO–C and MgO–T Nanoparticles

The XRD pattern of MgO–C nanoparticles (Fig. 4.5) shows characteristic diffraction peaks at 2θ values of 36.9°, 42.8°, 62.3°, 74.7°, and 78.6°, corresponding to the (111), (200), (220), (311), and (222) planes of cubic MgO. These peaks match well with standard MgO data (JCPDS card No. 45-0946), confirming the formation of crystalline magnesium oxide nanoparticles. The sharp diffraction peaks indicate good crystallinity, while slight peak broadening suggests nanoscale crystallite size in the range of 10–30 nm calculated using the Debye–Scherrer equation. The absence of impurity peaks confirms the phase purity of MgO–C nanoparticles [16]–[17].

Similarly, the XRD pattern of MgO–T nanoparticles (Fig. 4.6) exhibits diffraction peaks at 37.22°, 43.24°, 62.46°, 74.82°, and 78.78°, corresponding to the (111), (200), (220), (311), and (222) planes of cubic MgO structure. The peaks match with standard JCPDS card No. 45-0946, confirming face-centered cubic (FCC) MgO formation with lattice parameter a ≈ 4.21 Å. The crystallite size calculated using the Debye–Scherrer equation ranges from 13.1 to 29.7 nm, indicating nanocrystalline nature. No additional impurity peaks were observed, confirming high phase purity and successful green synthesis of MgO–T nanoparticles [16]–[17].

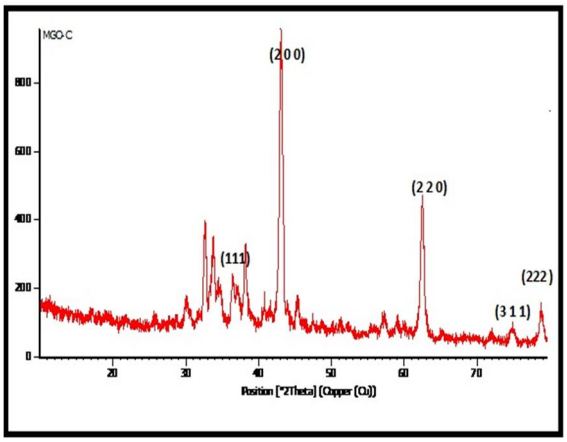

Fig 4.5 XRD Spectrum of MgO- C Nps

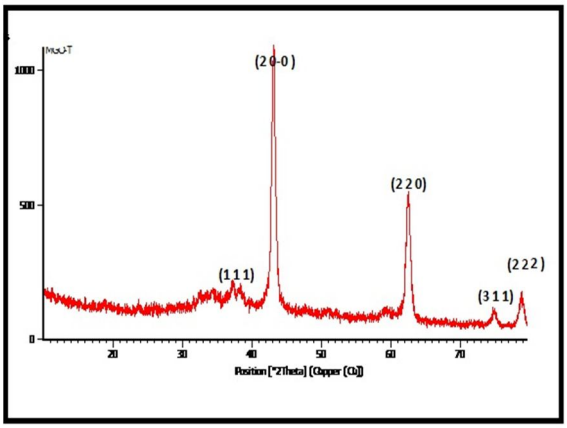

Fig 4.6 XRD Spectrum of MgO–T Nps

4) FESEM Analysis of MgO–C and MgO–T Nanoparticles

The FESEM micrograph of MgO–C nanoparticles (Fig. 4.7) reveals irregular to quasi-spherical shaped particles with noticeable agglomeration forming porous cluster structures. The particle size is estimated in the range of 30–70 nm, while aggregated clusters extend into the submicron scale due to high surface energy and phytochemical-mediated interactions during green synthesis. The rough and porous surface morphology indicates a large surface area beneficial for antimicrobial, catalytic, and adsorption applications. These features confirm the successful formation of nanoscale MgO–C nanoparticles [10]–[12].

Similarly, the FESEM image of MgO–T nanoparticles (Fig. 4.8) shows irregular to quasi-spherical particles with significant agglomeration forming porous micron-sized clusters. The particle size ranges from 40–80 nm, while aggregated clusters are observed in the range of **2–**8 µm. The porous and rough surface structure suggests enhanced surface area and improved functional properties. These morphological characteristics agree with previously reported plant-mediated MgO nanoparticles, confirming successful green synthesis of MgO–T nanoparticles [11]–[13].

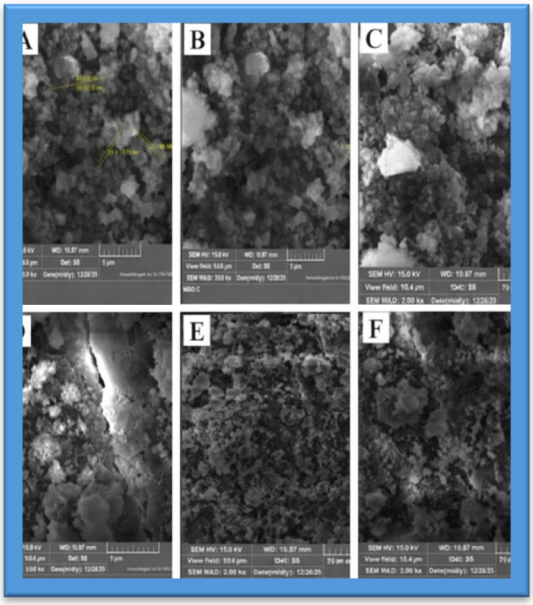

Fig 4.7 FESEM of MgO - C NPS

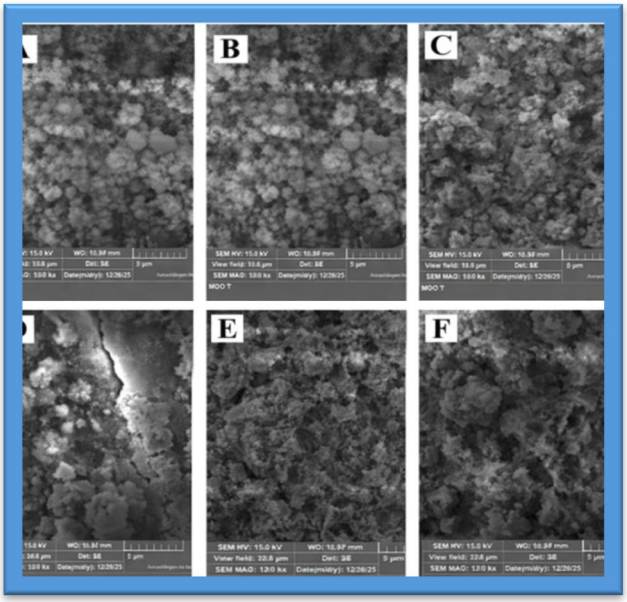

Fig 4.8 FESEM of MgO - T NPS

5) EDAX Analysis of MgO–C NPs

The EDAX spectrum of MgO–C nanoparticles (Fig. 4.9) confirms the elemental composition of magnesium oxide with strong peaks corresponding to oxygen and magnesium. The oxygen peak observed at approximately 0.52 keV corresponds to the O Kα transition, while the magnesium peak near 1.25 keV corresponds to the Mg Kα transition, confirming the formation of MgO nanoparticles. The absence of additional impurity peaks indicates high purity of the synthesized nanoparticles. The quantitative elemental composition of MgO–C nanoparticles is summarized in Table 4.1, and the results agree well with previously reported green synthesized MgO nanoparticles [16], [10], [11].

Similarly, the EDAX spectrum of MgO–T nanoparticles (Fig. 4.10) also shows strong peaks corresponding to oxygen and magnesium, confirming the formation of MgO nanoparticles. The peaks at ~0.52 keV (O Kα) and ~1.25 keV (Mg Kα**)** indicate the presence of MgO with high chemical purity. No additional impurity peaks were observed, confirming successful green synthesis of MgO–T nanoparticles. The quantitative elemental composition is presented in Table 4.2, and the results are consistent with earlier reports on plant-mediated MgO nanoparticles [16], [11], [13].

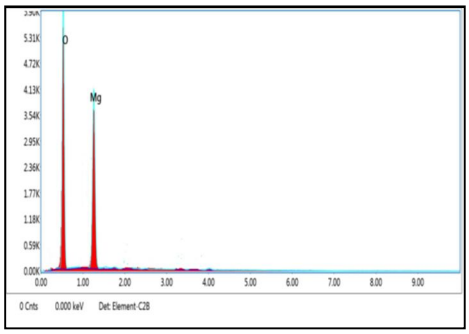

Fig 4.9 EDAX Spectrum of MgO- C NPS

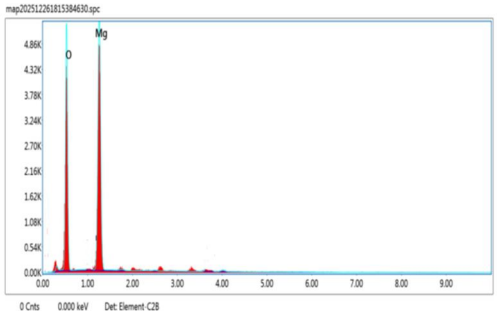

Fig 4.10 EDAX Spectrum of MgO- T NPS

Table 4.1 EDAX Elemental Analysis of MgO–C Nanoparticles

Element	Weight %	Atomic%	Net Int	Error %	Kratio	Z	A	F
O K	53.19	59.92	569.91	27.40	0.2988	3.6904	3.2063	4.0330
Mg K	46.81	40.08	589.71	12.60	0.2636	1.9307	1.1622	2.0035

Table 4.2 EDAX Elemental Analysis of MgO–T Nanoparticles

Element	Weight %	Atomic%	Net Int	Error %	Kratio	Z	A	F
O K	43.52	54.67	366.02	6.79	0.2327	1.0528	0.5080	1.0000

6) TG–DTG–DTA Analysis of MgO–C Nanoparticles

Thermogravimetric (TG–DTG–DTA) analysis of MgO–C nanoparticles was performed from room temperature to 900–1000 °C to evaluate thermal stability and decomposition behavior (Fig. 4.11 and Fig. 4.12). The TG curve shows multistep weight loss due to removal of moisture and decomposition of plant-derived organic compounds. The initial weight loss of about 8.0% below 250 °C is attributed to evaporation of physically adsorbed water and volatile constituents. A second weight loss of approximately 8.6% between 250 °C and 620 °C corresponds to decomposition of phytochemicals such as phenolics and flavonoids present on the nanoparticle surface. At higher temperatures (620–1000 °C), a gradual weight loss of about 6.8% is observed due to carbonization of residual organic matter [10], [11], [12].

The DTG curve shows a major decomposition peak around 350–380 °C, indicating breakdown of plant-derived biomolecules, while slow mass reduction above 400 °C corresponds to removal of residual carbonaceous material and crystallization of MgO. Beyond 700 °C, the mass remains nearly constant, confirming the formation of thermally stable MgO nanoparticles. The total weight loss of approximately 23–25% followed by stabilization indicates formation of thermally stable MgO residue suitable for high-temperature applications [10], [11], [12], [14].

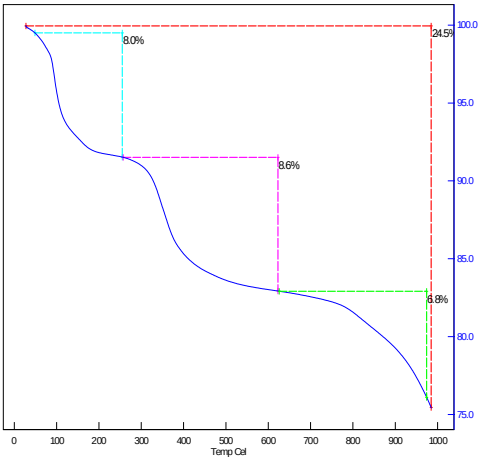

Fig 4.11 (TGA) Curve of MgO–C Nps

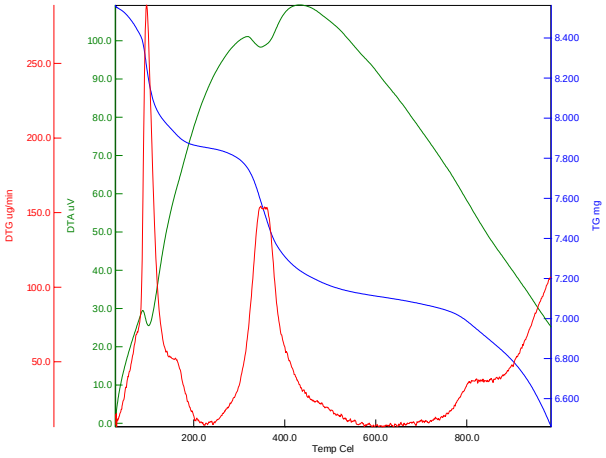

Fig 4.12 TG–DTG–DTA Curve of MgO–C Nps

7) TG–DTG–DTA Analysis of MgO–T Nanoparticles

Thermogravimetric (TG–DTG–DTA) analysis of MgO–T nanoparticles was carried out from room temperature to 900–1000 °C to evaluate thermal stability (Fig. 4.13 and Fig. 4.14). The TG curve shows multistep weight loss due to removal of moisture and decomposition of plant-derived organic compounds. An initial weight loss of about 4–5% below 120 °C is attributed to evaporation of adsorbed moisture and volatile components. A major weight loss of approximately 21.9% between 120 °C and 520 °C corresponds to thermal decomposition of phytochemicals such as phenolics and flavonoids present on the nanoparticle surface. Above 520 °C, a gradual weight loss of about 6.7% is observed due to carbonization of residual organic matter [10], [11], [12].

The DTG curve shows a prominent decomposition peak around 350–380 °C, indicating breakdown of plant-derived biomolecules. Further gradual mass loss above 400 °C corresponds to removal of residual carbonaceous matter and crystallization of MgO nanoparticles. The mass becomes nearly constant above 700 °C, confirming formation of thermally stable MgO nanoparticles suitable for high-temperature applications. The overall mass loss of approximately 30–33% followed by stabilization confirms successful green synthesis of thermally stable MgO–T nanoparticles [10], [11], [12], [13].

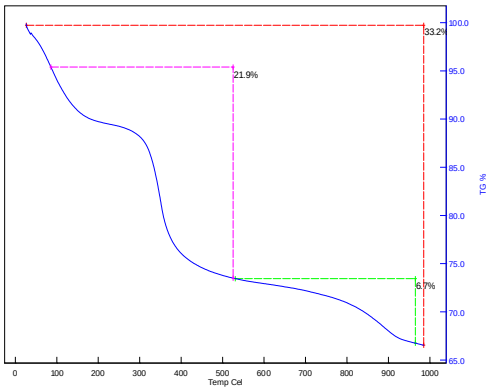

Fig 4.13 (TGA) Curve of MgO–T Nps

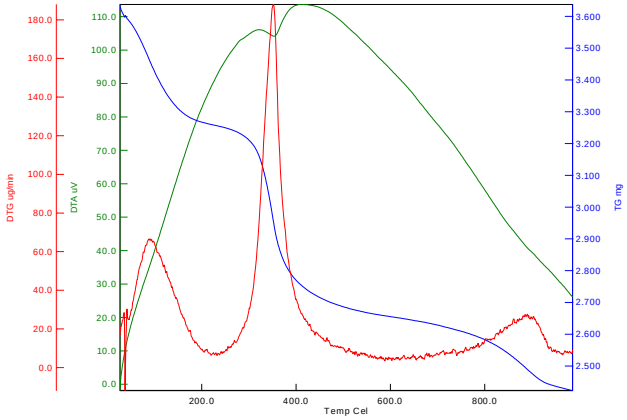

Fig 4.14 TG–DTG–DTA Curve of MgO–T Nps

B. Applications

1) Anti Bacterial Activity

The antibacterial activity of green-synthesized MgO–T and MgO–C nanoparticles was evaluated against selected Gram-positive and Gram-negative bacterial strains using the agar well diffusion method, and the results are presented in Table 4.3 and Fig. 5.15. The standard antibiotic ciprofloxacin showed higher inhibition zones compared to MgO nanoparticles, confirming the reliability of the experimental procedure. Both MgO–T and MgO–C nanoparticles exhibited moderate antibacterial activity, indicating their potential as eco-friendly antimicrobial agents, which is consistent with previously reported plant-mediated MgO nanoparticles showing similar antibacterial performance [10, 11].

Among the synthesized samples, MgO–C nanoparticles demonstrated comparatively higher antibacterial activity, with the maximum inhibition observed against *Bacillus cereus* (14 mm), while the lowest inhibition was recorded for *E. coli* (5 mm) in MgO–T nanoparticles. Gram-positive bacteria showed slightly higher sensitivity than Gram-negative bacteria due to differences in cell wall structure. The antibacterial activity of MgO nanoparticles is mainly attributed to reactive oxygen species generation, surface alkalinity, and membrane damage, which ultimately leads to bacterial cell death. Similar antibacterial mechanisms and activity trends for green-synthesized MgO nanoparticles have been reported in earlier studies, supporting the effectiveness of the synthesized nanoparticles for antimicrobial applications [10,11,12,13].

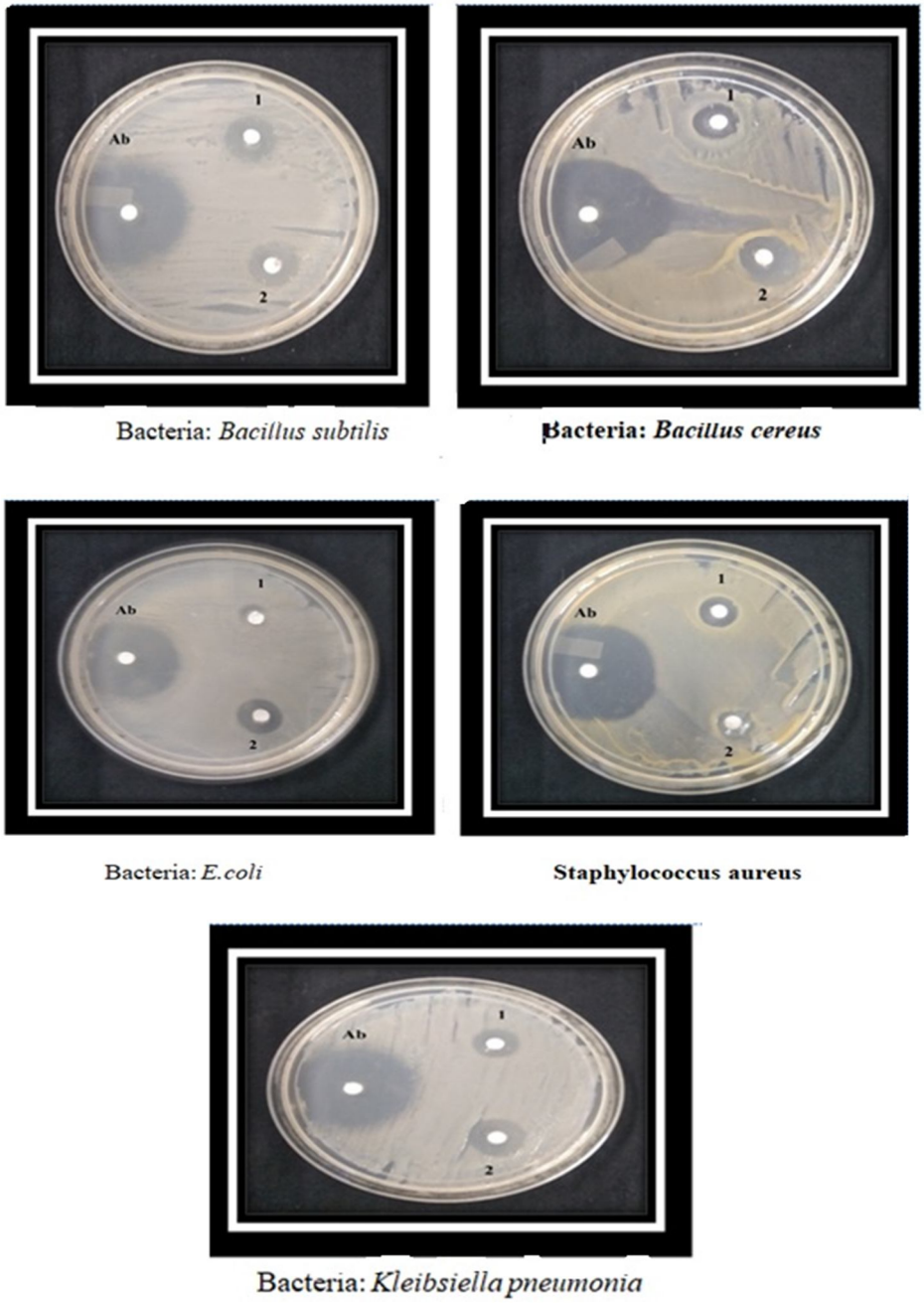

Fig 5.15 Antibacterialactivity

Table 4.3 Antibacterial Activity of MgO–T and MgO–C Nanoparticles Against Different Bacterial Strains

Bacteria	Inhibition zone in mm		
	Ab ciprofloxacin	1- MgO-T	2-MgO-C
E.coli	21	5	9
Staphylococcus aureus	27	8	8
Bacillus subtilis	25	11	12
Bacillus cereus	24	9	14
Kleibsiella pneumonia	25	9	10

2) Anti-Corrosion Activity

The anti-corrosion performance of MgO–T coated, MgO–C coated, and uncoated samples was evaluated using the weight loss method in acidic, basic, and neutral media, and the results are presented in Fig. 4.16. The uncoated sample exhibited the highest corrosion rate in all media, confirming severe metal dissolution, whereas MgO-based coatings significantly reduced corrosion due to their protective barrier effect. In acidic medium, the corrosion rate decreased from 4.9% (uncoated) to 2.1% for both MgO–T and MgO–C coatings, indicating effective protection against aggressive acidic conditions. Similarly, in basic medium, corrosion decreased from 4.6% to 2.2% and 2.0% for MgO–T and MgO–C coatings, respectively, showing improved coating stability, particularly for MgO–C nanoparticles.

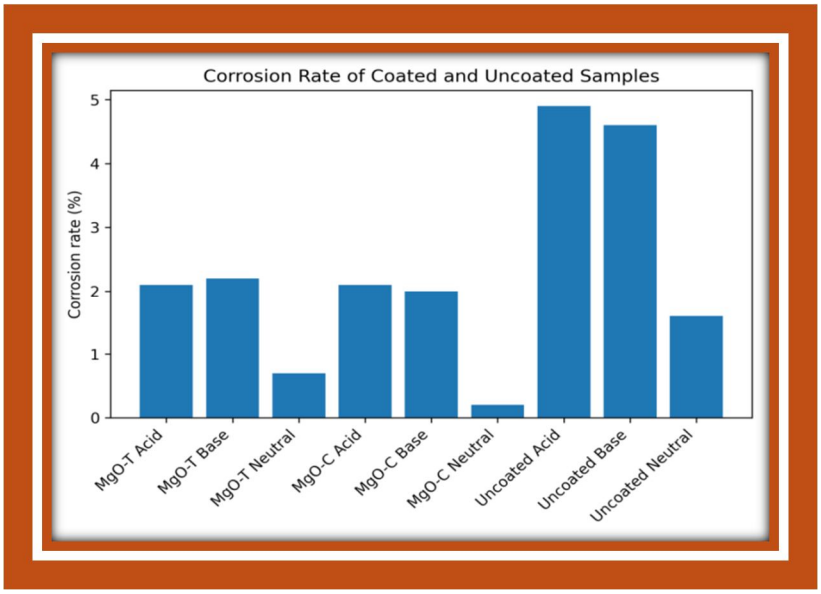

Fig 4.16 Image of Corrosion rate of Coated and uncoated samples

In neutral medium, MgO–C exhibited the lowest corrosion rate of 0.2%, followed by MgO–T (0.7%) and the uncoated sample (1.6%), confirming superior protective efficiency of MgO–C coating. The anti-corrosion efficiency followed the order MgO–C > MgO–T > Uncoated, demonstrating that MgO coatings significantly enhance corrosion resistance. The higher protection efficiency is attributed to the formation of a dense and uniform nanoparticle coating that prevents penetration of corrosive species. Similar corrosion inhibition behavior of MgO nanoparticle coatings has been reported in earlier studies, confirming their effectiveness as eco-friendly anti-corrosion materials for industrial applications (Fig. 4.17) [11], [12], [13].

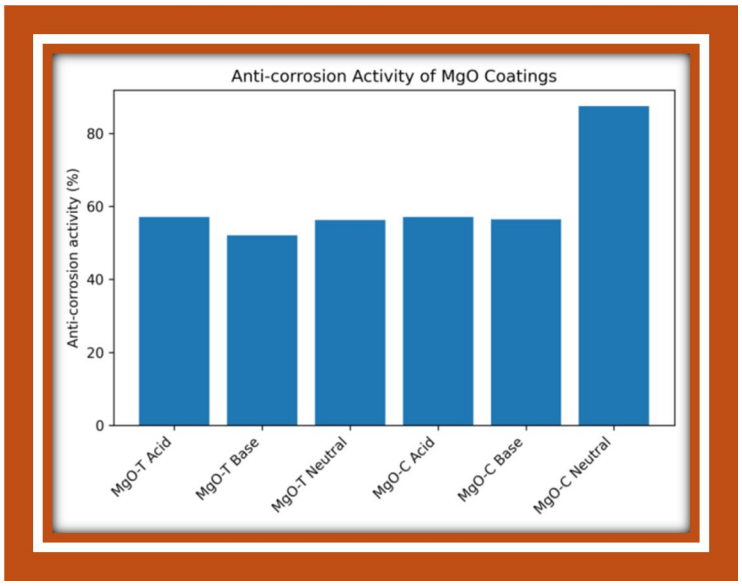

Fig 4.17 Image of Anti- Corrosion Activity of MgO Coatings

3) Shelf Life Time Extension Activity

The shelf-life study was carried out to evaluate the effectiveness of edible coating prepared using Terminalia arjuna bark extract on tomato preservation. Visual observations of coated and uncoated tomatoes were recorded on Day 1, Day 3, Day 5, and Day 7, as shown in Fig. 4.18. The coated tomatoes retained fresh appearance, smooth texture, and natural color throughout the storage period. Even on Day 7, only minimal surface changes were observed, indicating that the bioactive compounds in the bark extract formed a protective film that reduced moisture loss and slowed respiration, thereby delaying ripening and spoilage

In contrast, uncoated tomatoes showed rapid deterioration with visible dark spots appearing by Day 3, followed by wrinkling, fungal growth, and tissue softening by Day 5. The improved storage stability of coated tomatoes confirms that the antioxidant and antimicrobial phytochemicals present in the bark extract act as a semi-permeable barrier against microbial growth and moisture loss. Overall, the Terminalia arjuna bark extract coating significantly enhanced shelf life and maintained the post-harvest quality of tomatoes compared to uncoated samples (Fig. 4.18)

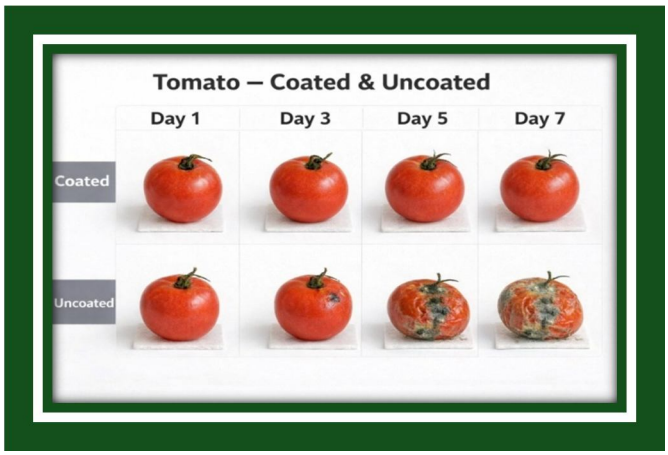

Fig 4.18 Image of Effect of *Terminalia arjuna bark* extract coating on the shelf life of Tomato

4) Coriandrum sativum Seed Extract Coating

The shelf-life study of capsicum was carried out to evaluate the effectiveness of edible coating prepared using Coriandrum sativum seed extract, and the observations are shown in Fig.4.19. The coated capsicum remained fresh, firm, and glossy for a longer storage period, maintaining its natural green color up to day 12 with only slight surface shrinkage. This improved preservation is attributed to the presence of bioactive compounds such as phenolics, flavonoids, and essential oils, which provide antioxidant and antimicrobial properties and form a protective film over the fruit surface.

In contrast, uncoated capsicum showed rapid deterioration with color change observed by day 6, followed by severe wrinkling, shrinkage, and softening by day 12. The enhanced shelf life of coated capsicum is due to the semi-permeable barrier formed by the coriander seed extract, which reduces moisture loss and slows respiration. Overall, Coriandrum sativum seed extract coating effectively improved shelf life and maintained post-harvest quality of capsicum compared to the uncoated control (Fig. 4.19).

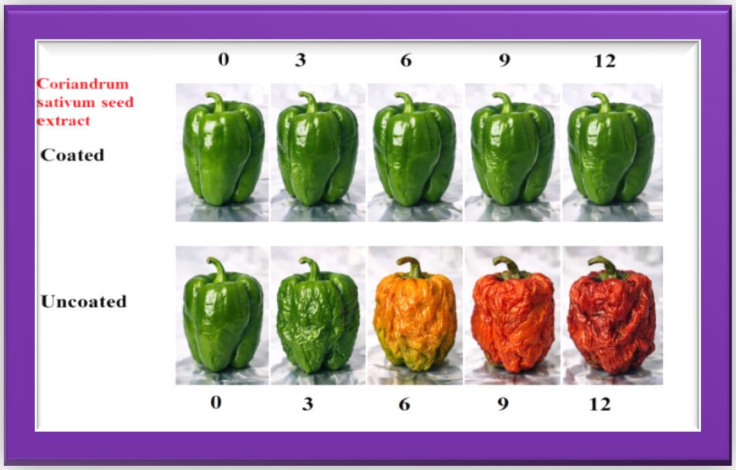

Fig 4.19 Image of Effect of *Coriandrum sativum seed* extract coating on the shelf life of capsicum

V. CONCLUSION

In this study, magnesium oxide nanoparticles were successfully synthesized through a green and eco-friendly approach using *Terminalia arjuna* bark extract (MgO–T) and *Coriandrum sativum* seed extract (MgO–C). The phytochemicals present in both plant extracts played a significant role as reducing, stabilizing, and capping agents, making the synthesis process simple, economical, and environmentally benign.

The formation of MgO nanoparticles was confirmed through various characterization techniques. UV–Visible spectroscopy exhibited characteristic absorption peaks in the range of 266–395 nm, confirming nanoparticle formation. FTIR analysis revealed the presence of functional groups such as O–H, C–H, C=O, and Mg–O vibrations, indicating the involvement of plant biomolecules in nanoparticle synthesis. XRD results confirmed the crystalline cubic structure of MgO nanoparticles, with MgO–T showing an average crystallite size of 20.4 nm and MgO–C exhibiting a comparatively larger size of 33 nm. SEM analysis demonstrated quasi-spherical to cubic shaped nanoparticles with slight agglomeration, while EDX spectra confirmed the elemental purity of magnesium and oxygen. TGA analysis indicated that both synthesized nanoparticles possessed good thermal stability up to 1000 °C.

The functional performance studies revealed that both MgO–T and MgO–C nanoparticles exhibited antibacterial activity, with MgO–C demonstrating comparatively higher inhibition efficiency. In corrosion studies, both coatings significantly reduced metal degradation, but MgO–C showed superior corrosion resistance. Furthermore, vegetable preservation studies indicated that MgO-coated capsicum samples maintained freshness for a longer duration than uncoated samples, with MgO–C again showing better preservation efficiency compared to MgO–T.

Overall, both green synthesized MgO nanoparticles exhibited promising structural, antibacterial, anti-corrosion, and food preservation properties. However, MgO–C nanoparticles demonstrated comparatively better performance in most of the evaluated parameters. Therefore, green synthesized MgO nanoparticles, particularly MgO–C, hold significant potential for applications in antimicrobial coatings, food preservation, corrosion protection, and environmental applications.

VI. ACKNOWLEDGEMENT

I would like to express my gratitude to my primary supervisor Dr.G.Savari Susila., 1, who guided me throughout this research article. I would also like to thank my friends and family who supported me and offered deep insight into the study.

REFERENCES

[1] S. Ahmed, M. Ahmad, B. L. Swami, and S. Ikram, “A review on plants extract mediated synthesis of silver nanoparticles for antimicrobial applications,” *Journal of Advanced Research*, vol. 7, no. 1, pp. 17–28, 2016. DOI: 10.1016/j.jare.2015.02.007

[2] S. Iravani, "Green synthesis of metal nanoparticles using plants," Green Chemistry, vol. 13, pp. 2638–2650, 2011. DOI: 10.1039/C1GC15386B
[3] A. K. Mittal, Y. Chisti, and U. C. Banerjee, "Synthesis of metallic nanoparticles using plant extracts," Biotechnology Advances, vol. 31, no. 2, pp. 346–356, 2013. DOI: 10.1016/j.biotechadv.2013.01.003
[4] J. Singh, T. Dutta, K. H. Kim, M. Rawat, P. Samddar, and P. Kumar, "Green synthesis of metals and their oxide nanoparticles: applications for environmental remediation," Journal of Nanobiotechnology, vol. 16, p. 84, 2018. DOI: 10.1186/s12951-018-0408-4
[5] K. Gopinath, S. Gowri, and A. Arumugam, "Phytosynthesis of gold nanoparticles using Terminalia arjuna bark extract and its application," Journal of Nanostructure in Chemistry, vol. 4, p. 115, 2014. DOI: 10.1007/s40097-014-0115-0
[6] V. Kumari, S. Kaushal, and P. P. Singh, "Green synthesis of CuO nanoparticles using Terminalia arjuna bark extract," Materials Advances, vol. 3, pp. 2170–2184, 2022. DOI: 10.1039/D1MA00993A
[7] B. Laribi, K. Kouki, M. M'Hamdi, and T. Bettaieb, "Coriander (Coriandrum sativum L.): phytochemistry and biological activities," European Food Research and Technology, vol. 241, pp. 1–16, 2015. DOI: 10.1007/s00217-015-2441-8
[8] C. Sreelakshmi et al., "Green synthesis of metal nanoparticles using plant extracts and their biomedical applications," Environmental Research, vol. 204, p. 112298, 2021. DOI: 10.1016/j.envres.2021.112298
[9] M. Nasrollahzadeh, S. M. Sajadi, and Z. Issaabadi, "Green nanotechnology: synthesis of metal nanoparticles using plant extracts," Chemical Record, vol. 19, no. 12, pp. 2436–2479, 2019. DOI: 10.1002/tcr.20190009
[10] S. Iravani, "Green synthesis of metal nanoparticles using plants," Green Chemistry, vol. 13, pp. 2638–2650, 2011.
[11] J. Singh, T. Dutta, K. H. Kim, M. Rawat, P. Samddar, and P. Kumar, "Green synthesis of metals and their oxide nanoparticles," Journal of Nanobiotechnology, vol. 16, 2018.
[12] M. Nasrollahzadeh, S. M. Sajadi, M. Sajjadi, and Z. Issaabadi, "Green synthesis of metal nanoparticles using plant extracts," Journal of Colloid and Interface Science, vol. 497, pp. 1–27, 2017.
[13] F. Al-Hazmi and A. Al-Ghamdi, "Optical properties of MgO nanoparticles," Ceramics International, vol. 38, pp. 5715–5720, 2012.
[14] M. A. Gondal, T. F. Qahtan, and M. A. Dastageer, "Synthesis and characterization of MgO nanoparticles," Applied Surface Science, vol. 256, pp. 298–304, 2010.
[15] S. Ahmed, M. Ahmad, B. L. Swami, and S. Ikram, "Green synthesis of nanoparticles using plant extracts," Journal of Advanced Research, vol. 7, pp. 17–28, 2016.
[16] B. D. Cullity and S. R. Stock, Elements of X-Ray Diffraction, 3rd ed., Prentice Hall, 2001.
[17] W. L. Bragg, "Crystal structure," Nature, vol. 105, pp. 646–648, 1920.

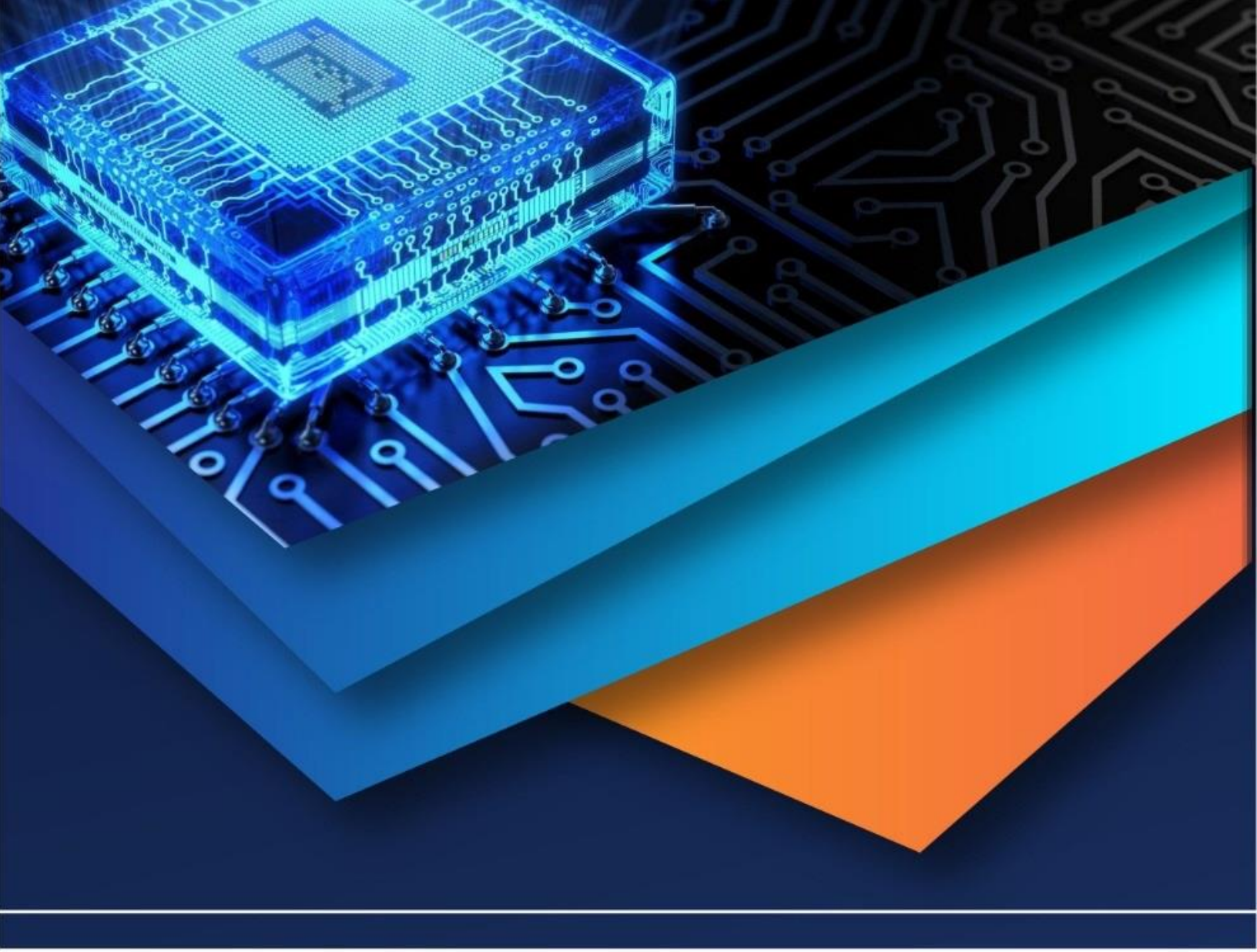

10.22214/IJRASET

45.98

IMPACT FACTOR: 7.129

IMPACT FACTOR: 7.429

INTERNATIONAL JOURNAL FOR RESEARCH

IN APPLIED SCIENCE & ENGINEERING TECHNOLOGY